Oxidation reactions on neutral cobalt oxide clusters: experimental and theoretical studies

Yan Xie,[a] Feng Dong,[a] Scott Heinbuch,[b] Jorge J. Rocca[b] and Elliot R. Bernstein*[a]

Received 30th July 2009, Accepted 23rd October 2009
First published as an Advance Article on the web 26th November 2009
DOI: 10.1039/b915590b

Reactions of neutral cobalt oxide clusters (Co_mO_n, m = 3–9, n = 3–13) with CO, NO, C_2H_2, and C_2H_4 in a fast flow reactor are investigated by time of flight mass spectrometry employing 118 nm (10.5 eV) single photon ionization. Strong cluster size dependent behavior is observed for all the oxidation reactions; the Co_3O_4 cluster has the highest reactivity for reactions with CO and NO. Cluster reactivity is also highly correlated with either one or more following factors: cluster size, Co(III) concentration, the number of the cobalt atoms with high oxidation states, and the presence of an oxygen molecular moiety (an O–O bond) in the Co_mO_n clusters. The experimental cluster observations are in good agreement with condensed phase Co_3O_4 behavior. Density functional theory calculations at the BPW91/TZVP level are carried out to explore the geometric and electronic structures of the Co_3O_4 cluster, reaction intermediates, transition states, as well as reaction mechanisms. CO, NO, C_2H_2, and C_2H_4 are predicted to be adsorbed on the Co(II) site, and react with one of the parallel bridge oxygen atoms between two Co(III) atoms in the Co_3O_4 cluster. Oxidation reactions with CO, NO, and C_2H_2 on the Co_3O_4 cluster are estimated as thermodynamically favorable and overall barrierless processes at room temperature. The oxidation reaction with C_2H_4 is predicted to have a very small overall barrier (<0.23 eV). The oxygen bridge between two Co(III) sites in the Co_3O_4 cluster is responsible for the oxidation reactions with CO, NO, C_2H_2, and C_2H_4. Based on the gas phase experimental and theoretical cluster studies, a catalytic cycle for these oxidation reactions on a condensed phase cobalt oxide catalyst is proposed.

Introduction

Transition metal oxides (TMOs) are widely used as heterogeneous catalysts or catalysis supports in the chemical industry.[1,2] Gold based catalysts are employed for low temperature CO oxidation,[3] and have been studied extensively in the condensed phase[4–10] and in the gas phase,[11–14a] but a search for alternative, low-cost, and noble metal free materials has led to the study of transition metal and metal oxide catalysts[15–41] for such reactions. Catalysts containing cobalt metal and metal oxides are very important for low temperature carbon monoxide oxidation,[24–41] nitrogen monoxide reduction and oxidation,[24,36a,42–44] and Fischer–Tropsch reactions.[45,46] Co_3O_4 and CoO are the most stable stoichiometric structures for all cobalt oxide species; CoO can be generated by heating Co_3O_4 at high temperature (~900 °C).[47] Co_3O_4 has a spinel structure, including two Co(III) ions and one Co(II) ion in the Co_3O_4 unit to balance the four oxygen atomic charges. Co_3O_4 is found to be the active site for low temperature CO oxidation.[28,30,31,37,38] For Co_3O_4 supported by Al_2O_3[26,27a,b]/CeO_2[29,33,40,41]/ZrO_2,[36b] reactions for CO oxidation to CO_2 occur even at temperatures below 0 °C. Most studies of cobalt oxide catalysts are focused on condensed phase systems: the catalysts are characterized by X-ray diffraction (XRD) and X-ray photoelectron spectroscopy (XPS), and catalytic reactions are investigated by temperature programmed desorption (TPD), temperature programmed reduction and oxidation (TPR and TPO), infrared spectroscopy (IR), thermogravimetric analysis (TGA), mass spectrometry (MS), and by other techniques, as well.

Reaction mechanisms for carbon monoxide oxidation on cobalt oxide catalysts are still unclear even through many efforts have been focused on this issue. Only a very simple mechanism for the low temperature CO oxidation has been proposed: CO is adsorbed on an oxidized cobalt site [Co(II) or Co(III)], reacts with surface oxygen to form CO_2, and CO_2 is readily desorbed from the surface. For example, Jansson *et al.* have studied CO oxidation over Co_3O_4/Al_2O_3 by using isotope labeled $^{18}O_2$ and have found that one of the oxygens of the CO_2 molecule comes from the catalyst surface, and the reduced cobalt can be re-oxidized by the gas phase oxygen, or can be further reduced (deactivated) by another CO molecule.[27]

Several critical questions for the detailed mechanism are still open; different groups have drawn opposite conclusions from the available data, however. Jansson *et al.* suggest that CO is probably adsorbed on a Co(III) site based on Fourier transform infrared spectrometry (FT-IR): they observe an IR band

[a] *Department of Chemistry, NSF ERC for Extreme Ultraviolet Science and Technology, Colorado State University, Fort Collins, CO 80523, USA. E-mail: erb@lamar.colostate.edu*
[b] *Department of Electrical and Computer Engineering, NSF ERC for Extreme Ultraviolet Science and Technology, Colorado State University, Fort Collins, CO 80523, USA*

at 2164 cm^{-1}.[27] On the other hand, CO is suggested to be adsorbed on the Co(II) and Co(III) sites by Pollard *et al.*, employing the same method.[37] A band centered at 2006 cm^{-1} is assigned to CO linearly adsorption on a Co(II) site; the adsorbed CO reacts with an oxygen atom bonded to a neighboring Co(III) to form CO_2. In this process, Co(III) is reduced to Co(II). The catalytic activity highly depends in this instance on the specific ratio of Co(II)/Co(III) and particle size. The catalyst can be regenerated by reaction of Co(II) with O_2 to re-oxidize the cobalt atom: a reaction mechanism is proposed,[37] but the adsorption site is difficult to identify experimentally [Co(III) or Co(II)] by Co 2p XPS spectra, because the binding energy difference between Co(III) and Co(II) is small (only 0.9 eV).[36b] Subsequently, density functional theory (DFT) calculations performed to study CO oxidation on the Co_3O_4 (110) surface predict that CO adsorbs on a Co(III) site on the top surface layer with the carbon atom bound to the surface and the molecular axis parallel to the surface normal direction. This binding energy is calculated to be 1.7 eV. CO_2 is formed through a structure in which the carbon atom of CO is bonded to both the Co(III) and a neighboring oxygen atom.[28] Luo *et al.* have proposed that at least two kinds of oxygen species exist on the Co_3O_4/CeO_2 surface: one is very active for low temperature CO oxidation, and the other is mainly active for high temperature CO oxidation.[40] A catalytic cycle is suggested in which CO oxidation occurs at the interface between Co_3O_4 and CeO_2, involving the surface O_2^- radical ion species. Wang *et al.* have suggested that O_2^- and O^- are the active oxygen species on the Co_3O_4 surface, on the basis of their O_2-TPD experiments.[38] All the assumed mechanisms focus on the interface between Co_3O_4 with the support; no reaction mechanisms are proposed for oxidation of CO to CO_2 on pure Co_3O_4 condensed phase surfaces or clusters even through high catalytic reactivity is observed for a pure Co_3O_4 catalyst.

Clusters in the gas phase can be good model systems to simulate real surface reactions and to discover surface reaction mechanisms: clusters are readily accessible by theoretical techniques because they are isolated and their properties are localized. Published studies on Co containing clusters deal mostly with pure metal charged and neutral clusters, reacting with CO, O_2, H_2, CH_3OH, *etc.*[11b,48–62] For cobalt oxide clusters, electronic and geometric structures for neutral and anionic CoO_n (n = 1–4) clusters have been reported by Uzunova *et al.*, and a dissociation channel, loss of a dioxygen molecule, is suggested based on their DFT calculations.[63] In addition, $Co_mO_n^-$ (m = 4–20, n = 0–2) anion clusters are generated by a laser ablation source and are investigated by photoelectron spectroscopy.[64] Electron binding energies for each $Co_mO_n^-$ cluster are determined experimentally. Recently, cationic and anionic cobalt oxide clusters ($Co_mO_n^{\pm}$, m = 1–3, n = 1–6) have been studied with regard to their reactions with CO by guided ion beam mass spectrometry and DFT calculations; only anionic clusters have reactivity toward CO oxidation.[14b] Neutral, cationic, and anionic cluster reactions are investigated experimentally and theoretically to explore catalytic mechanisms, understand catalytically active sites, and improve catalytic processes in the condensed phase. These clusters represent tractable model systems through which detailed catalytic behavior can be explored and elucidated. Once the cluster reactions are understood through experiment and theory, predictions and suggestions can be offered for improving the condensed phase catalytic activity. Both neutral and ionic cluster behavior can be important in this modeling process; if predictions for condensed phase behavior are borne out, the models are useful.

In our present studies, neutral cobalt oxide clusters are generated by laser ablation, reacted with CO, NO, C_2H_2, and C_2H_4 in a fast flow reactor, and reactants and products are detected by time of flight mass spectrometry (TOFMS). Ionization of these neutral species occurs through absorption of single photon, vacuum ultra-violet (VUV) laser radiation (118 nm, 10.5 eV per photon). The isolated products CO_2, NO_2, CH_2CO, and CH_3CHO are not observed in the mass spectra. CO_2 has an ionization energy of 13.78 eV, which is higher than the 10.5 eV (118 nm) single photon energy. The ionization energies of NO_2, CH_2CO, and CH_3CHO are lower than 10.5 eV; however, their concentrations in the molecular beam are too low to detect. Based on the original Co_3O_4 concentration, cross sections for collisions, and reaction cross section estimates, we expect the signal for these species to be quite small (<0.1 mV) and thus not above the threshold for detection. Non-fragmenting ionization by a 118 nm laser has been successfully applied for the studies of the reactions of transition metal oxide clusters, and the results have been reported recently.[65] DFT calculations are further performed to explore the reaction mechanisms for the Co_3O_4 cluster and, through comparison between gas phase cluster results and condensed phase catalytic reactions, a mechanism is suggested for the catalytic oxidation of CO to CO_2 on a Co_3O_4 condensed phase surface.

Experimental procedures

Reactions of neutral cobalt oxide clusters with CO, NO, C_2H_2, and C_2H_4 are investigated by TOFMS coupled with single photon ionization (SPI) as described in detail in previous publications.[65a–c] Only a brief outline of the experiment is given below. Cobalt oxide clusters are generated in a laser ablation source: cobalt plasma, ablated from a cobalt foil disk, reacts with oxygen seeded in helium (10% O_2/He) expansion gas. A focused, second harmonic (532 nm) beam from a Nd^{3+}:YAG laser, with a 10 Hz repetition rate and 7 mJ per pulse energy, is used for laser ablation. The expansion gas is pulsed into the vacuum by a supersonic nozzle (R. M. Jordan, Co.) with a backing pressure of typically 70 psi. Generated cobalt oxide clusters react with appropriate reactants (CO, NO, C_2H_2, and C_2H_4) in a fast flow reactor (i.d. 6.3 mm × 76 mm), directly coupled with the cluster generation channel (i.d. 1.8 mm × 19 mm). The reactant gases, seeded in 20 psi helium gas, are injected into the reactor by a pulsed General Valve (Parker, Series 9). The timing between the Jordan valve and the General Valve openings is optimized for the best product yields. The pressure in the fast flow reactor can be estimated as 14 Torr for the reaction and the collision rate between cobalt oxide clusters and helium is estimated *ca.* 10^8 s^{-1}.[65b] Reactants and products are thermalized to 300–400 K by collision after the reaction.[66]

All ions are removed from the molecular beam by an electric field located downstream from the reactor. Charge transfer and neutralization in the fast flow reactor has been addressed completely in the literature: the small amount of ionic species that might be present in the beam does not influence the abundant neutral cluster distributions or reactions.[65c] Only neutral species, including reactants, reaction intermediates, and products are skimmed into a differentially pumped vacuum chamber and ionized by a single photon of VUV 118 nm laser light. 118 nm laser radiation is generated by focusing the third harmonic of a Nd^{3+}:YAG laser (355 nm, ~30 mJ per pulse) into a tripling cell containing *ca.* 250 Torr argon/xenon gas mixture (10 : 1). A MgF_2 prism (Crystaltechno LTD, Russia, 6° apex angle) is placed into the laser beam to increase separation of the generated 118 nm laser beam from the 355 nm input laser beam. The intensity of the 118 nm laser is *ca.* 1 μJ cm^{-2} and the photon energy is 10.5 eV, which is higher than most of the transition metal oxide vertical ionization energies (8–10 eV). After the near threshold ionization, photoions are detected by a TOFMS, and the signals are amplified and recorded by a digital storage oscilloscope.

Calculational procedures

The structural parameters for neutral cobalt oxide clusters and their reaction intermediates, transition states, and products with CO, NO, C_2H_2, and C_2H_4 are calculated by DFT. All the calculations are carried out with Becke's exchange[67] and Perdew–Wang[68] correlation functional coupled with a triple-ζ valence plus polarization (TZVP) basis set within the Gaussian 03 program.[69] The calculations for the potential energy surfaces (PESs) of the reactions of cobalt oxide with CO, NO, C_2H_2, and C_2H_4, involve geometry optimizations of the reactants, intermediates, transition states, and products. Vibrational frequency calculations are further performed to confirm the global minima ground states and transition states, which have zero and one imaginary frequency, respectively. Additionally, intrinsic reaction coordinate (IRC) calculations are carried out to determine that an estimated transition state connects two appropriate local minima along reaction pathways.

Results and discussion

1. Mass spectrum of neutral cobalt oxide clusters

Fig. 1 presents a typical TOF mass spectrum of neutral cobalt oxide Co_mO_n (m = 2–11, n = 3–16) clusters generated by a laser ablation source, and ionized by 118 nm laser radiation. The 10% oxygen in the helium carrier gas is higher than that employed for generation of Ti_mO_n, V_mO_n, Fe_mO_n, Zr_mO_n, Nb_mO_n, and Cu_mO_n[65] but does give the best distribution of Co_mO_n clusters. In Fig. 1, the most intense mass peaks for each cobalt series are located at Co_3O_3, Co_4O_4, Co_5O_5, Co_5O_6, Co_6O_9, Co_7O_{10}, Co_8O_{11}, Co_9O_{12}, $Co_{10}O_{13}$, $Co_{10}O_{14}$, and $Co_{11}O_{15}$. The relatively high signal intensities are at $n = m$ for m = 3–5, $n = m + 3$ for m = 6–10, and $n = m + 4$ for m = 10–11. The neutral cobalt oxide cluster distribution is different from the anion $Co_mO_n^-$ distribution:[64] the ion intensities are in the sequence $Co_mO^- > Co_m^- > Co_mO_2^- > Co_mO_3^-$ for the anionic cobalt oxide clusters. Because only pure helium, without added oxygen, is used as the expansion gas for $Co_mO_n^-$ generation, observation of more oxygen-deficient clusters (Co_mO_n, $n < m$) than in the spectrum presented in Fig. 1 might be a reasonable expectation. In other anionic cluster studies, 10% O_2 seeded in helium is used for cluster generation, and $CoO_{2,3}^-$, $Co_2O_{3-5}^-$, $Co_3O_{4-6}^-$, $Co_4O_{6,7}^-$, and $Co_5O_{6-9}^-$ are observed as the dominant clusters.[14b]

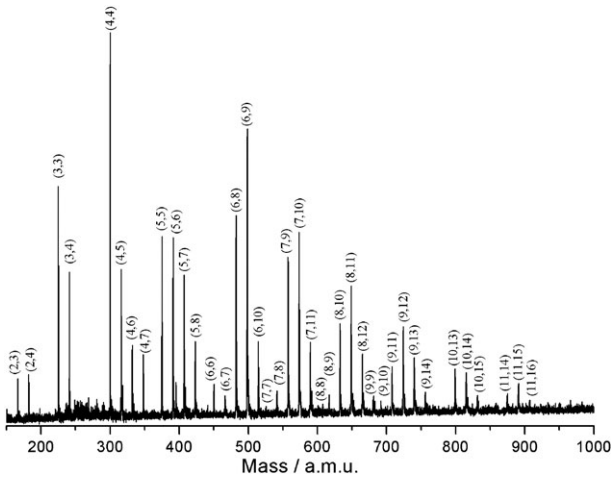

Fig. 1 Neutral cobalt oxide cluster Co_mO_n (m = 2–11, n = 3–16) distribution detected by 118 nm single photon ionization and time of flight mass spectrometry.

2. Reaction of neutral cobalt oxide clusters with CO

5% CO seeded in helium gas is employed for the reaction of Co_mO_n with CO in a fast flow reactor, and the product distribution is presented in Fig. 2. Mono-adsorption products, $Co_3O_{3-4}CO$, $Co_4O_{4-5}CO$, $Co_5O_{6-7}CO$, $Co_6O_{8-9}CO$, *etc.* are observed for the most intense cobalt oxide clusters. In addition, the biggest change is that the signals for all the observed Co_mO_n clusters are decreased after the reaction with CO in the fast flow reactor. This reactant signal decrease can be attributed to both clusters scattering from the molecular beam by collisions in the reactor, and reactions between CO and cobalt oxide clusters for the CO oxidation: $Co_mO_n + CO \rightarrow Co_mO_{n-1} + CO_2$. The scattering effect is difficult to evaluate directly in our experiments; however, it is larger, generally, for larger clusters, since they have larger scattering cross sections. A reference scattering experiment with 5% inert C_3H_8 in He in the fast flow reactor shows that all cobalt oxide cluster signals decrease *ca.* 10% uniformly upon passing the cluster beam through the reactor cell. We conclude, therefore, that the non reactive scattering effect is negligible for the decrease of reactant signals. The reaction contribution is much larger than the scattering effect: for example, the Co_3O_4 signal decreases 87% after reaction with CO in Fig. 2. The decrease signals indicate the reactions $Co_mO_n + CO \rightarrow Co_mO_nCO \rightarrow Co_mO_{n-1} + CO_2$, for example, $Co_3O_4 + CO \rightarrow Co_3O_4CO \rightarrow Co_3O_3 + CO_2$, occur in the reactor.

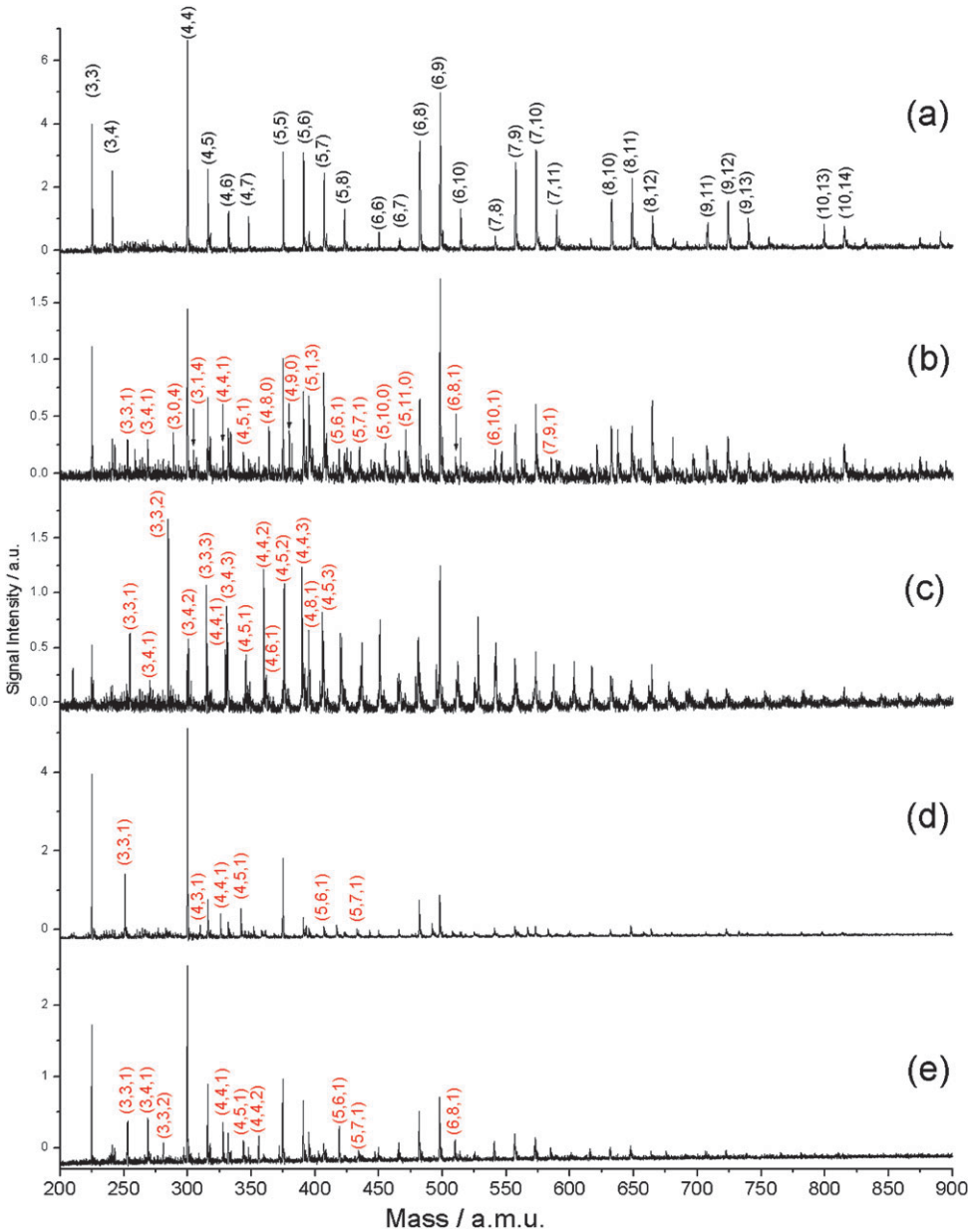

Fig. 2 Neutral cobalt oxide cluster distributions after reaction and collision with (a) pure helium; (b) 5% CO/He; (c) 5% NO/He; (d) 5% C_2H_2/He; and (e) 5% C_2H_4/He in a fast flow reactor. Products are labeled as $Co_mO_nX_y$ (m, n, y, X = CO, NO, C_2H_2, and C_2H_4). See text for details.

Overall reaction rate constants for the reaction of Co_mO_n with CO are calculated as previously described and listed in Table 1.[65n] The parameters adopted for rate constant calculations are P (pressure) = 14 Torr, t (cluster reaction time) = 76 mm/1500 m s^{-1} = 51 μs, T (temperature) = 350 K, and A (collision rate with CO, NO, C_2H_2, and C_2H_4) = 5% × 10^8 s^{-1} = 5 × 10^6 s^{-1}. Note that the overall rate constants are calculated based on the signal intensity decrease of the reactants, which contributes to both direct association and subsequent oxidation reactions. As discussed in the literature,[65b] the reaction intermediates, $Co_mO_nCO^*$, can either surmount a reaction barrier to form Co_mO_{n-1} + CO_2, or be cooled to form products Co_mO_nCO by collision with the bath gas. As shown in Fig. 2, some association products, such as $Co_3O_{3-4}CO$, $Co_4O_{4-5}CO$, $Co_5O_{6-7}CO$ and $Co_6O_{8,10}CO$, are observed when CO is added in the fast flow reactor; however, compared to the overall intensity decrease of the reactant signals, less than 10% of the signal decrease is due to the intermediate association reactions. For example, the intensity of Co_3O_4CO signal is only *ca.* 10% of the intensity of unreacted Co_3O_4 original signal. Therefore, the decrease of the reacting cluster intensities is due mainly to oxidation reactions since reduction reactions are not thermodynamically favorable. Some cobalt oxide clusters, such as $Co_4O_{8,9}$, $Co_5O_{10,11}$, which are not observed in collision with pure helium in Fig. 2(a), are detected in the reaction with CO in Fig. 2(b). Apparently strong size dependent behavior is observed for all the cobalt oxide clusters. The Co_3O_4 cluster has the largest reaction rate constant, 1.62 × 10^{-12} cm^3 s^{-1}, of any Co_mO_n cluster. Other relatively large rate constants are

Table 1 Experimentally derived rate constants for reaction of cobalt oxide clusters Co_mO_n (m,n) with CO, NO, C_2H_2, and C_2H_4

Clusters	Rate constants/10^{-12} cm^3 s^{-1} [a]			
	CO	NO	C_2H_2	C_2H_4
(3,3)	1.01	3.15	0.72	0.10
(3,4)	1.62	4.02	2.08	2.30
(4,4)	1.21	3.79	1.03	0.50
(4,5)	1.02	2.86	1.13	1.24
(4,6)	0.81	2.26	0.84	0.89
(4,7)	1.42	3.78	1.50	1.75
(5,5)	0.86	3.59	1.21	0.75
(5,6)	1.10	3.02	1.37	1.81
(5,7)	0.75	2.75	1.91	1.89
(5,8)	1.29	3.2	2.59	1.94
(6,6)	0.92	1.19	1.25	1.41
(6,7)	0.18	0.19	0.87	1.15
(6,8)	1.23	3.33	1.43	1.20
(6,9)	0.81	2.02	1.31	1.17
(6,10)	0.91	2.82	1.60	1.70
(7,8)	0.27	0.17	1.06	1.25
(7,9)	1.31	2.47	1.87	2.20
(7,10)	1.19	2.57	2.16	2.37
(7,11)	1.33	2.64	3.13	2.71
(8,9)	0.47	0.26	0.88	1.55
(8,10)	0.87	2.15	2.20	2.20
(8,11)	1.15	2.76	2.55	2.30
(8,12)	0.28	1.09	1.84	1.40
(9,11)	0.66	1.52	2.22	2.32
(9,12)	0.98	2.53	2.99	1.79
(9,13)	0.94	2.21	3.22	2.01

[a] The absolute error in the values of the rate constants is *ca.* 50% based on an estimate of the average concentration of reactants in the fast flow reactor. The relative error for the rate constants is less than 10% based on signal intensity variation from different experiments. See ref. 65*b*.

observed for Co_4O_7, Co_5O_8, Co_6O_8, Co_7O_{11}, Co_8O_{11}, and Co_9O_{12}, with rate constants of 1.42, 1.29, 1.23, 1.33, 1.15, and 0.98 × 10^{-12} cm^{3}s^{-1}, respectively.

For each given m in Co_mO_n clusters, the calculated rate constants vary, but not in a simple, linear fashion. This behavior is related to the concentration of Co(III) or Co(II) in the Co_mO_n clusters and the following general, qualitative trends can be identified. First, $(Co_3O_4)_n$ (n = 1, 2, 3) clusters have relatively high reaction rate constants for a given m in Co_mO_n clusters, and the Co_3O_4 cluster has the highest reaction rate constant. This behavior for these clusters can be explained by the appropriate Co(III) concentration [Co(III)/(Co(III) + Co(II)) = 0.67] and their small particle size compared to the larger reactive Co_mO_n clusters. Second, clusters with only Co(II), such as Co_3O_3, Co_4O_4, Co_5O_5, and Co_6O_6 (Co_mO_m, m = 3–6), and clusters with only Co(III), such as Co_4O_6, Co_6O_9, and Co_8O_{12}, or generally $(Co_2O_3)_n$ (n = 2–4), have relatively low reaction rate constants compared with Co_mO_n clusters of the same m value. The reduced reactivity of these clusters is related to their Co(III) concentrations (0 and 1), which are quite different from 0.67 for $(Co_3O_4)_n$ (n = 1, 2, 3) clusters. Third, some oxygen rich clusters, such as Co_4O_7, Co_5O_8, Co_6O_{10}, and Co_7O_{11}, have relatively high rate constants for a given m in Co_mO_n clusters. Fourth, the rate constants for other Co_mO_n clusters, including Co_4O_5, Co_5O_{6-7}, CO_6O_8, Co_7O_{8-10}, Co_8O_{9-11}, Co_9O_{11}, and Co_9O_{13} depend on the difference of their Co(III)/Co(II) ratios compared to that for Co_3O_4 (0.67). For example, the Co(III) concentration ratios decrease in the order Co_3O_4 (0.67), Co_4O_5 (0.5), Co_5O_6 (0.4), Co_6O_7 (0.33), Co_7O_8 (0.29), and Co_8O_9 (0.25), and their rate constants are generally in the order Co_3O_4 > Co_4O_5, Co_5O_6 > Co_6O_7, Co_7O_8, Co_8O_9. These experimental rate constants do not exactly match with each Co(III) concentration due to the uncertainty in their values.[65b] Note that the Co_6O_7 cluster has a lower reaction rate constant than the Co_6O_6 cluster, which does not follow the above trends.

For some oxygen-rich gas-phase clusters, Co_4O_7, Co_5O_8, Co_6O_{10}, and Co_7O_{11}, even with all the cobalt atoms in a +3 oxidation state, the total oxygen charge [n × (−2)] cannot be balanced. Therefore, either some cobalt atoms must have a high oxidation state (+4 or +5) or O–O bonding (Co_mO_{n-2}–O_2) must exist for these oxygen rich cobalt oxide clusters, similar to that found for some V_mO_n clusters.[65m,70] Structures of oxygen rich Co_mO_n clusters can be predicted by theoretical calculations. For example, three conformers of the neutral Co_4O_7 cluster, which is an oxygen rich cluster, are explored by DFT and presented in Fig. 3. Both Conformer A and Conformer C are predicted to have the same lowest energy. One of the cobalt atoms has a +5 oxidation state and the other three cobalt atoms have a +3 oxidation state in Conformer A, whereas a Co–O–O–Co group structure exists in Conformer C. Conformer B is higher in energy than Conformers A and C by 0.42 eV, and has an O_2 molecule weakly bonded to two cobalt atoms. The O–O moiety binding energies for Conformers B and C are calculated at 1.71 and 2.30 eV. The average bond lengths between oxygen atoms in the O–O bonded moiety and Co(III) sites for Conformers B and C are estimated at 1.993 and 1.770 Å; therefore, the O–O moiety is more weakly bonded in Conformer B than that in Conformer C. The reaction Co_4O_7 + CO → Co_4O_6 + CO_2 could be attributed to either the reduction of Co(V) to Co(III) or loss of an oxygen atom from the Co–O–O–Co group, since Conformer A and C are the most stable structures for the Co_4O_7 cluster. For other oxygen rich clusters such as Co_5O_8, Co_6O_{10}, and Co_7O_{11}, *etc.*, the mechanism for the CO to CO_2 oxidation will depend on the cluster structure. If the cluster structure is similar in form to Co_4O_7 Conformer A, then the Co atom in the clusters will be reduced from a +4 or +5 oxidation state to a +3 oxidation state. If the cluster structures are similar to those for Co_4O_7 Conformers B and C with O–O bonded moieties, then the Co–O–O–Co or oxo bond will contribute to the oxidation of CO to CO_2.

Studies of condensed phase cobalt oxide catalysts have found:[29,41] 1. high levels of adsorbed O_2 are important for the CO to CO_2 conversion process; 2. high oxygen content systems tend to be unstable; and 3. high oxygen content catalysts Co_mO_{n+x} are easily reduced to Co_mO_n with only Co(II) and Co(III) species; and 4. the low temperature oxidation of CO by a cobalt oxide catalyst can be associated with the reduction of Co(III) to Co(II) in the Co_mO_n catalyst.[37] Reported studies[37] indicate that the reactivity of cobalt oxide catalysts with only Co(II) or Co(III) is lower than that of catalysts with a mixture of Co(II) and Co(III): an appropriate ratio of Co(III)/Co(II) is important for high catalytic activity of Co_mO_n low temperature CO oxidation.[37] Additionally, this

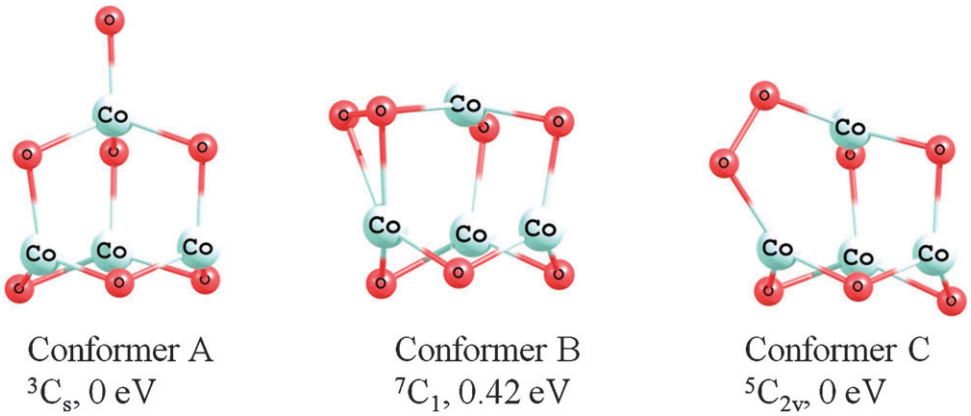

Fig. 3 Three conformer structures of Co_4O_7 cluster estimated at the BPW91/TZVP level of theory. The ^3C_s Conformer A and $^5C_{2v}$ Conformer B structures have the same energy within 0.005 eV.

reactivity can be improved by lowering the particle size for the Co_mO_n catalyst, as this increases the catalyst surface area.

In summary, high catalytic reactivities or large reaction rate constants for Co_mO_n clusters reacting with CO (see Table 1) are related to small cluster size, appropriate Co(III) concentration, the number of cobalt atoms with high oxidation states, and the possible presence of O–O bonding in cobalt oxide clusters. These conclusions for gas phase clusters are consistent with observations and results for condensed phase catalytic systems.

Since Co_3O_4 has the highest reactivity toward CO oxidation for the studied cobalt oxide clusters, the PES for the reaction of Co_3O_4 with CO is calculated at the BPW91/TZVP level of theory and shown in Fig. 4. The Co_3O_4 cluster has C_{2v} symmetry with doublet and quartet spin multiplicities: the doublet conformer is slightly higher in energy than the quartet conformer by 0.10 eV. DFT calculations predict bond lengths of 1.761 Å for Co(II)–O and 1.801 Å for Co(III)–O in $^2Co_3O_4$, with two parallel oxygen bridges between two Co(III) atoms. The product Co_3O_3 has a C_s symmetry, with the doublet conformer slightly higher in energy than the quartet conformer by 0.10 eV. As seen in the Co_3O_4 cluster spin density profile in Fig. 5, electrons are mostly localized on the Co(II) site, which is the most active site in the Co_3O_4 cluster. The lowest energy conformer structure for the association product Co_3O_4CO has the CO bonded to the Co(II) site; this structure is lower in energy than the conformer with CO bound to a Co(III) site by 0.23 eV. Additionally, since Co(II) is a more electron rich site than Co(III), CO bonding to a Co(II) site is reasonable according to the well established metal carbonyl chemistry. The calculated result is different from that of ref. 28, for which CO is suggested to be adsorbed on a Co(III) site based on a condensed phase surface approximation using a different DFT approach. The CO stretch energy is estimated at 2047 cm^{-1} for the Co_3O_4CO cluster based on our DFT calculations, and considering a reasonable scale factor of 0.9794 for the BPW91 method,[71] the adjusted energy of 2005 cm^{-1} is in good agreement with the experimental results (2006 cm^{-1}) and conclusions of ref. 37. The C–O bond length of 1.151 Å is slightly longer than that of the CO molecule, 1.138 Å as calculated. The 5σ lone pair electrons of the CO molecule interact with d orbitals of the Co(II). π back donation from the Co(II) to the CO is also confirmed by molecular orbital plots. Both interactions reduce the C–O bond electron density. The Co(II)–C bond length is estimated at 1.781 Å. Other conformers for this association species, O atom bound to the Co(II), C atom bound to the Co(III), and O atom bound to the Co(III) are higher in energy than the above lowest energy conformer by 1.40, 0.23, 1.50 eV, respectively. The association energies are calculated as 1.33 eV for both doublet and quartet conformers, which are lower than the 1.7 eV estimated previously.[28] CO_2 is formed linearly on the Co_3O_4 cluster through a transition state **TS1** (−0.52 eV for the doublet and −0.45 eV for the quartet), indicating that the CO molecule attacks one of the parallel bridge oxygen atoms between the two Co(III) atoms. The transition state **TS1** involves cleavage of two Co(III)–O bonds and elongation of the Co(II)–C bond. The overall reaction $Co_3O_4 + CO \rightarrow Co_3O_3 + CO_2$ is exothermic (−2.16 eV for the doublet and −2.27 eV for the quartet), and thermodynamically barrierless.

From the spin density profile for Co_3O_4CO in Fig. 5, electrons are localized at two Co (III) atoms and bridge oxygen atoms for the intermediate complexes **I1**. Therefore the bridge oxygen atoms are responsible for the high reactivity of the Co_3O_4 cluster for CO oxidation. Generally, for CO oxidation, one oxygen atom in CO_2 is from the bridge oxygen connected to two Co(III) atoms, and these two Co(III)s are reduced to Co(II)s in the product Co_3O_3.

The calculational results presented in Fig. 4 support the conclusions reached by FT-IR studies, that CO is adsorbed on the Co(II) site.[37] In addition, our calculated oxidation process also agrees with ref. 28: the added oxygen to CO is from one of the O atoms bound to the Co(III) site, as confirmed for the condensed phase systems experimentally and theoretically.

In summary, our experimental results agree with condensed phase studies as follows: 1. small clusters have large rate constants for CO oxidation in the gas phase in agreement with condensed phase observation; 2. CO is predicted to adsorb on a Co(II) site, in agreement with condensed phase IR data; 3. the CO oxidation reaction is calculated as a thermodynamically favorable process in agreement with the low temperature oxidation behavior of the cobalt oxide catalyst; 4. the oxygen atom for CO to CO_2 oxidation is proposed to come from the cobalt oxide surface, rather than the dissociated oxygen molecules based on theoretical

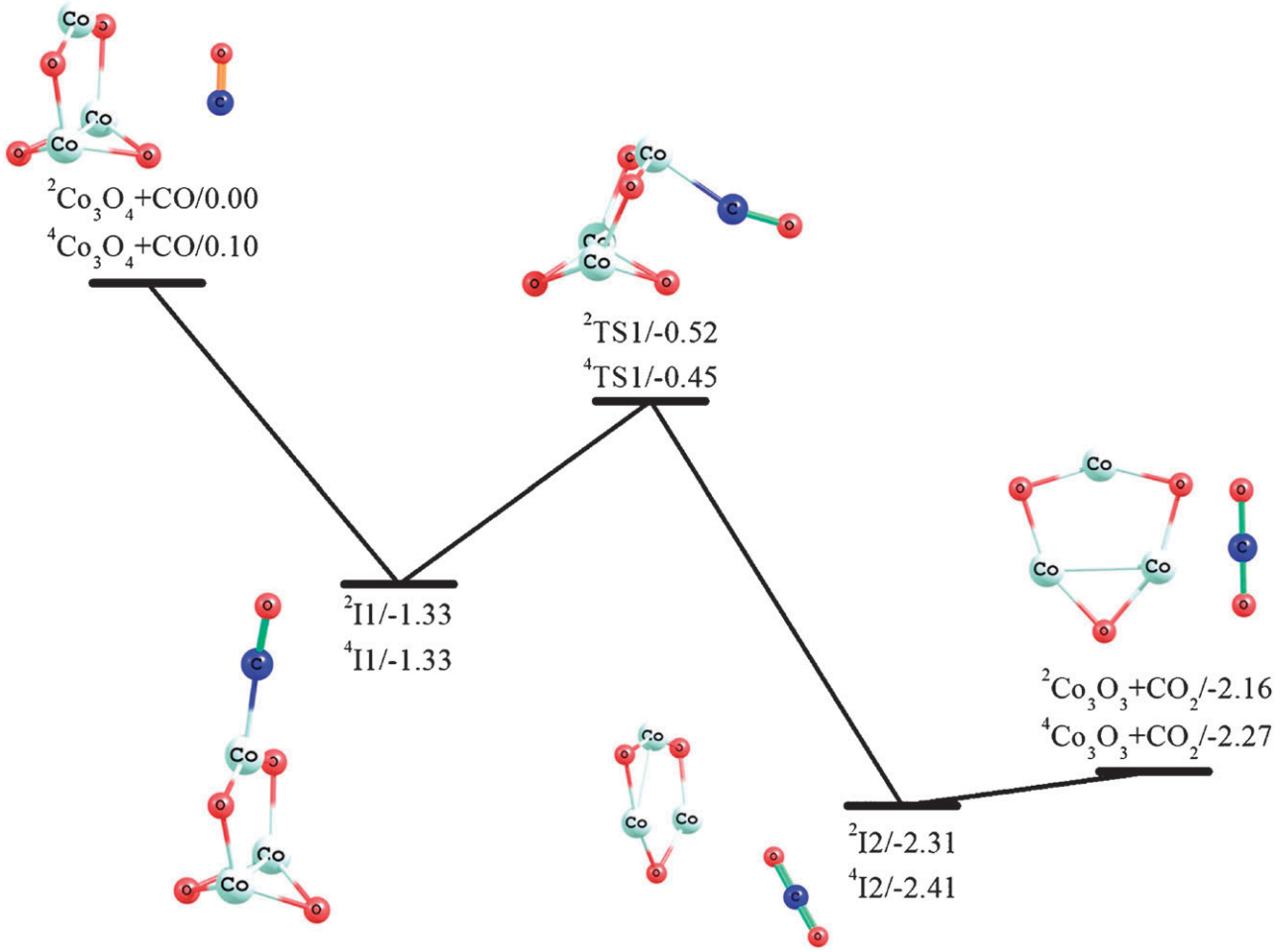

Fig. 4 Reaction pathway for $^{2/4}Co_3O_4 + CO \rightarrow {}^{2/4}Co_3O_3 + CO_2$ calculated at the BPW91/TZVP level. The reaction intermediates and transition states are denoted as $^M I_n$ and $^M TS_n$, respectively, in which the superscript M indicates the spin multiplicity. Energies, including ZPE corrections, are given in eV and are relative to the initial energy of the $^2Co_3O_4 + CO$ reactants. Cobalt atoms are the lightest in colour, followed by oxygen, and carbon as the darkest.

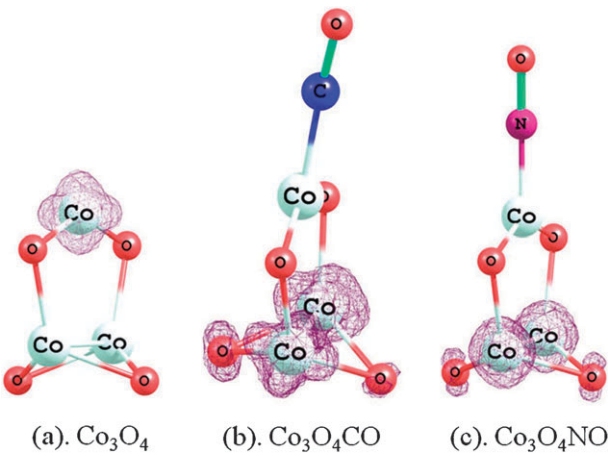

Fig. 5 Spin density profiles for Co_3O_4, Co_3O_4CO, and Co_3O_4NO clusters.

calculations, in agreement with the condensed phase isotopic experimental results; and 5. $(Co_3O_4)_n$ clusters have relatively high reactivity compared to other clusters which have one more or less oxygen atom. This latter point agrees with the condensed phase conclusions that 1. the Co_3O_4 crystal and Co_3O_4 supported by $Al_2O_3/CeO_2/ZrO_2$ exhibit catalytic reactivity toward CO oxidation, and 2. pure Co_2O_3 and CoO do not have such catalytic activity.

3. Reaction of neutral cobalt oxide clusters with NO

Reactions of neutral cobalt oxide clusters with 5% NO/He in the fast flow reactor are investigated as shown in Fig. 2(c) and the calculated reaction rate constants are listed in Table 1. The overall rate constants for reaction with NO are larger than those for reaction with CO by a factor of *ca.* 2.5. Generally, the rate constants decrease as cluster size increases. The Co_3O_4 cluster exhibits the largest rate constant (4.02×10^{-12} cm^3 s^{-1}) for the reactions of Co_mO_n with NO, and $(Co_3O_4)_x$ (x = 2,3) clusters have relatively larger rate constants compared to others for the given value of m (*e.g.* m = 6 and 9).

The overall reaction $Co_3O_4 + NO \rightarrow Co_3O_3 + NO_2$ is an exothermic process (−0.03 eV for the doublet Co_3O_3 and −0.14 eV for the quartet Co_3O_3), with a reaction barrier of −1.08 eV, as shown in Fig. 6. The lowest energy structure

for the $^5Co_3O_4NO$ reaction intermediate has C_{2v} symmetry and a quintet spin multiplicity, with the NO molecular axis parallel to the Co_3 (Co(II)–Co(III)–Co(III)) plane. The association energy is calculated to be −1.67/−2.05/−2.12 eV for singlet/triplet/quintet Co_3O_4NO, respectively, which is much higher than that for Co_3O_4–CO. The bond length of Co(II)–N is estimated at 1.649 Å, which is slightly shorter than the Co(II)–C bond length of 1.781 Å, as the interaction of Co–N is stronger than that for Co–C. NO_2 is formed on the Co_3O_4 cluster through transition state **TS2**, in which the N atom of NO attacks one of the bridge oxygen atoms between the two Co(III) atoms. The transition state structure **TS2** is similar to the structure **TS1** for the reaction with CO. Similar to the spin density profile for Co_3O_4CO, the profile for Co_3O_4NO indicates that the bridge oxygen atoms are the active site for the NO oxidation reaction, as shown in Fig. 5.

For CO and NO oxidation reactions, the Co_3O_4 cluster has the highest reaction rate, and $(Co_3O_4)_n$ (n = 2, 3) clusters have relatively high reaction rates. The structure of Co_3O_4 is unique because a parallel oxygen bridge between two Co(III) exists. Other calculated clusters, including Co_3O_3, Co_4O_5, Co_4O_6, and Co_4O_7, do not have such a feature. The spin density profiles for Co_3O_4CO and Co_3O_4NO indicate that the oxygen bridge is the active site for both CO and NO oxidation reactions.

4. Reaction of neutral cobalt oxide clusters with C_2H_2 and C_2H_4

The overall reaction rate constants for C_2H_2 and C_2H_4 oxidation on neutral cobalt oxide clusters are listed in Table 1, and the PESs for reactions $Co_3O_4 + C_2H_2 \rightarrow Co_3O_3 + CH_2CO$ and $Co_3O_4 + C_2H_4 \rightarrow Co_3O_3 + CH_3CHO$ are explored at the BPW91/TZVP level and shown in Fig. 7 and 8, respectively.

Similar to the reactions discussed above, obvious size dependent behavior is observed for both C_2H_2 and C_2H_4 oxidation; however, the Co_3O_4 cluster, or more generally $(Co_3O_4)_n$ (n = 1, 2, 3) clusters, are not the global maxima for the reactivity. In these reactions the rate constants increase with increasing cluster size. These rate constant profiles are opposite to those for CO and NO reactions with Co_mO_n. The reactivity for C_2H_2 and C_2H_4 oxidation increases with increasing Co(III) concentration for a given m value in a Co_mO_n cluster, except for the clusters only involving Co(III). The rate

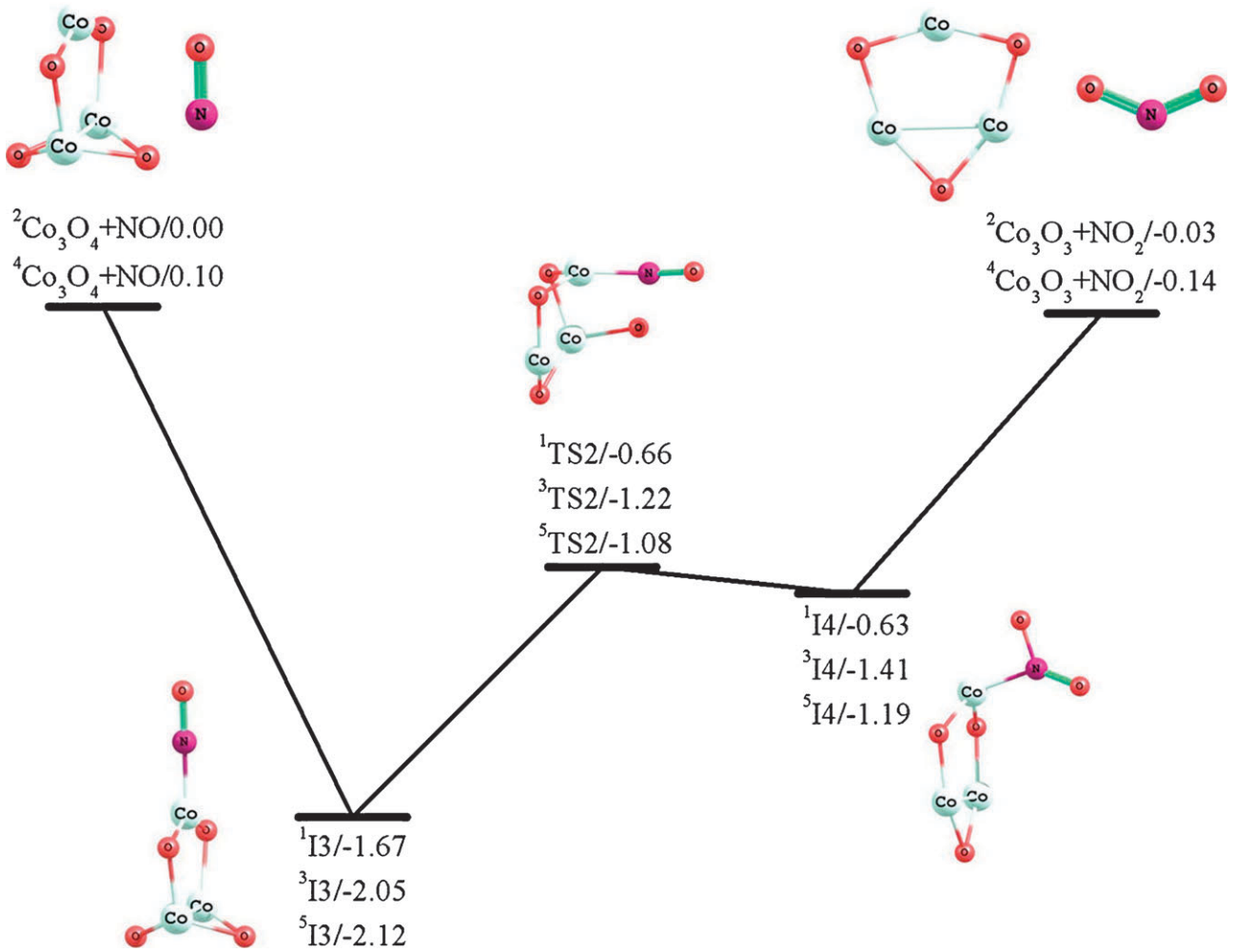

Fig. 6 Reaction pathway for $^{2/4}Co_3O_4 + NO \rightarrow {}^{2/4}Co_3O_3 + NO_2$ calculated at the BPW91/TZVP level. See caption to Fig. 4 for explanation. All the energies are relative to the initial energy of the $^2Co_3O_4$ + NO reactants.

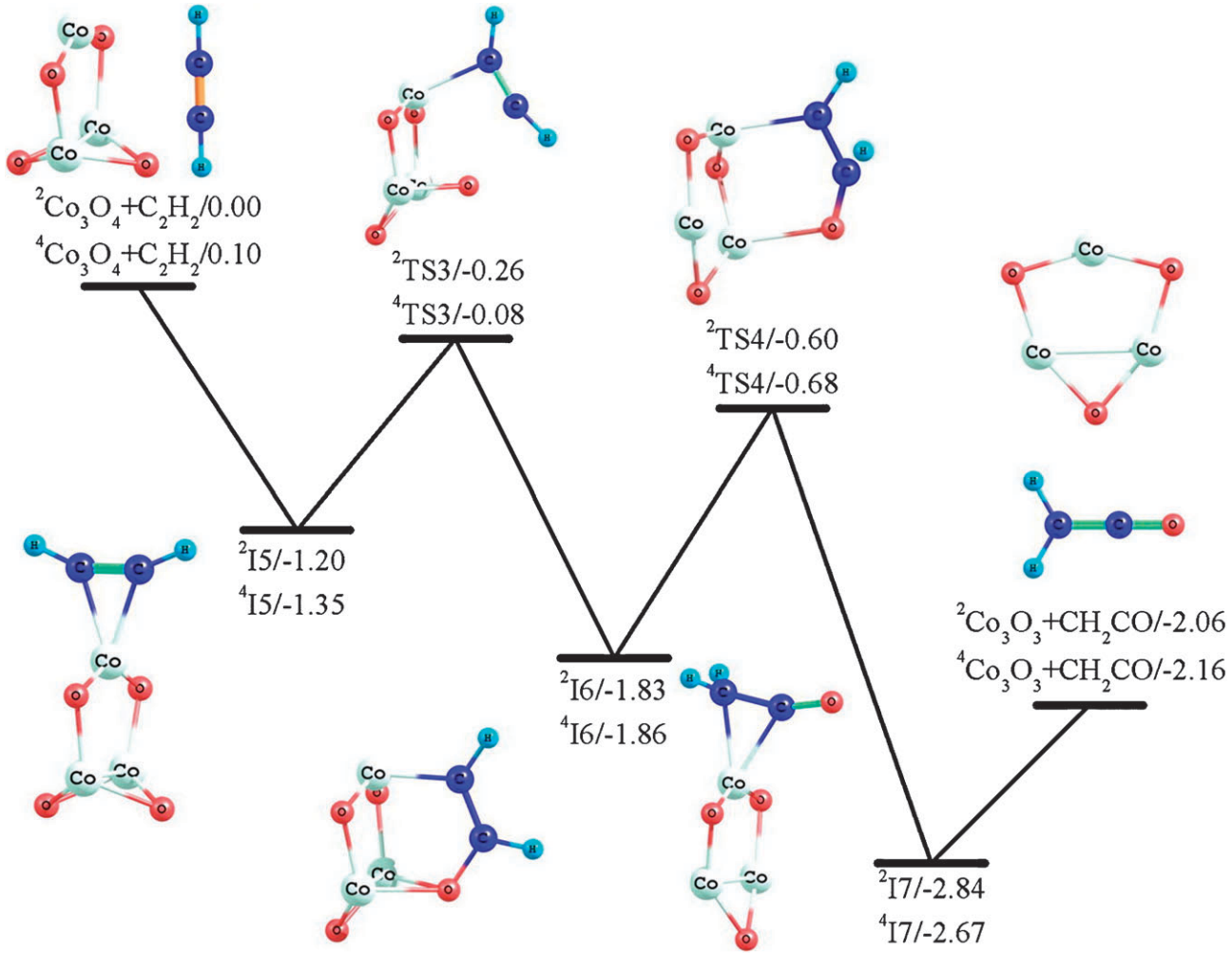

Fig. 7 Reaction pathway for $^{2/4}Co_3O_4 + C_2H_2 \rightarrow {}^{2/4}Co_3O_3 + CH_2CO$ calculated at the BPW91/TZVP level. See caption to Fig. 4 for explanations. All the energies are relative to the initial energy of the $^2Co_3O_4 + C_2H_2$ reactants.

constants are relatively low for clusters $(Co_2O_3)_n$ (n = 2, 3, 4). Additionally, clusters with structures associated with high cobalt oxidation states or O–O bonding moieties exhibit the highest reactivity for a given m value in the Co_mO_n clusters (*e.g.* Co_4O_7, Co_5O_8, Co_6O_{10}, and Co_7O_{11}). High reactivity for unsaturated hydrocarbons (C_2H_2 and C_2H_4) is notably related to large cluster size, high Co(III) concentration (but not equal to 1), more cobalt atoms with high oxidation states, or the presence of more O–O bonding in the Co_mO_n clusters.

The reaction $Co_3O_4 + C_2H_2 \rightarrow Co_3O_3 + CH_2CO$ is predicted to be exothermic with reaction energies −2.06 eV for the doublet and −2.16 eV for the quartet Co_3O_3 product (see Fig. 7). Two transition states, **TS3** (a C atom of C_2H_2 approaching an O atom of the bridge oxygen atoms between the two Co(III) species) and **TS4** (hydrogen transfer between the two C atoms to form CH_2CO), are lower in energy than the initial reactant structure $^2Co_3O_4 + C_2H_2$ by 0.26/0.08 and 0.60/0.68 eV, respectively. C_2H_2 is adsorbed onto the Co(II) site in Co_3O_4 through interaction of the π orbital of C_2H_2 with the Co(II), with association energy of 1.20/1.35 eV for doublet/quartet $Co_3O_4C_2H_2$, respectively. The interaction of the triple C–C bond with Co(II) weakens the triple bond, elongating it from 1.208 Å in the molecule to 1.261 Å in the adsorption structure ^{2}**I5**. The axis of the triple bond of C_2H_2 is perpendicular to the Co_3 plane (Co(II)–Co(III)–Co(III)). A reaction intermediate **I6**, with a cage structure in which two carbon atoms are bonded to Co(II) and oxygen bridge, is formed through transition state **TS3**. Subsequently, one hydrogen transfers from the carbon atom connected to the oxygen atom to the other carbon atom through **TS4**, and the CH_2CO species is formed on the Co(II) site and dissociated, as shown in Fig. 7.

Similarly, CH_3CHO is generated on the Co_3O_4 cluster through reaction with C_2H_4 as shown in Fig. 8. The C_2H_4 molecule adsorbs to the Co(II) site of the Co_3O_4 cluster with its double bond axis perpendicular to the Co_3 plane, in a structure similar to that of $Co_3O_4C_2H_2$. This adsorption also elongates the C=C bond length from 1.333 Å to 1.402 Å in $Co_3O_4C_2H_4$. Through a transition state **TS5** incorporating a bridge oxygen atom and a transition state **TS6** for hydrogen transfer between the two carbon atoms, a CH_3CHO moiety is formed and adsorbed onto the Co(III) site through an oxygen. Transition states **TS5** and **TS6** for C_2H_4 oxidation are higher in energy than **TS3** and **TS4** for C_2H_2 oxidation, and slightly higher

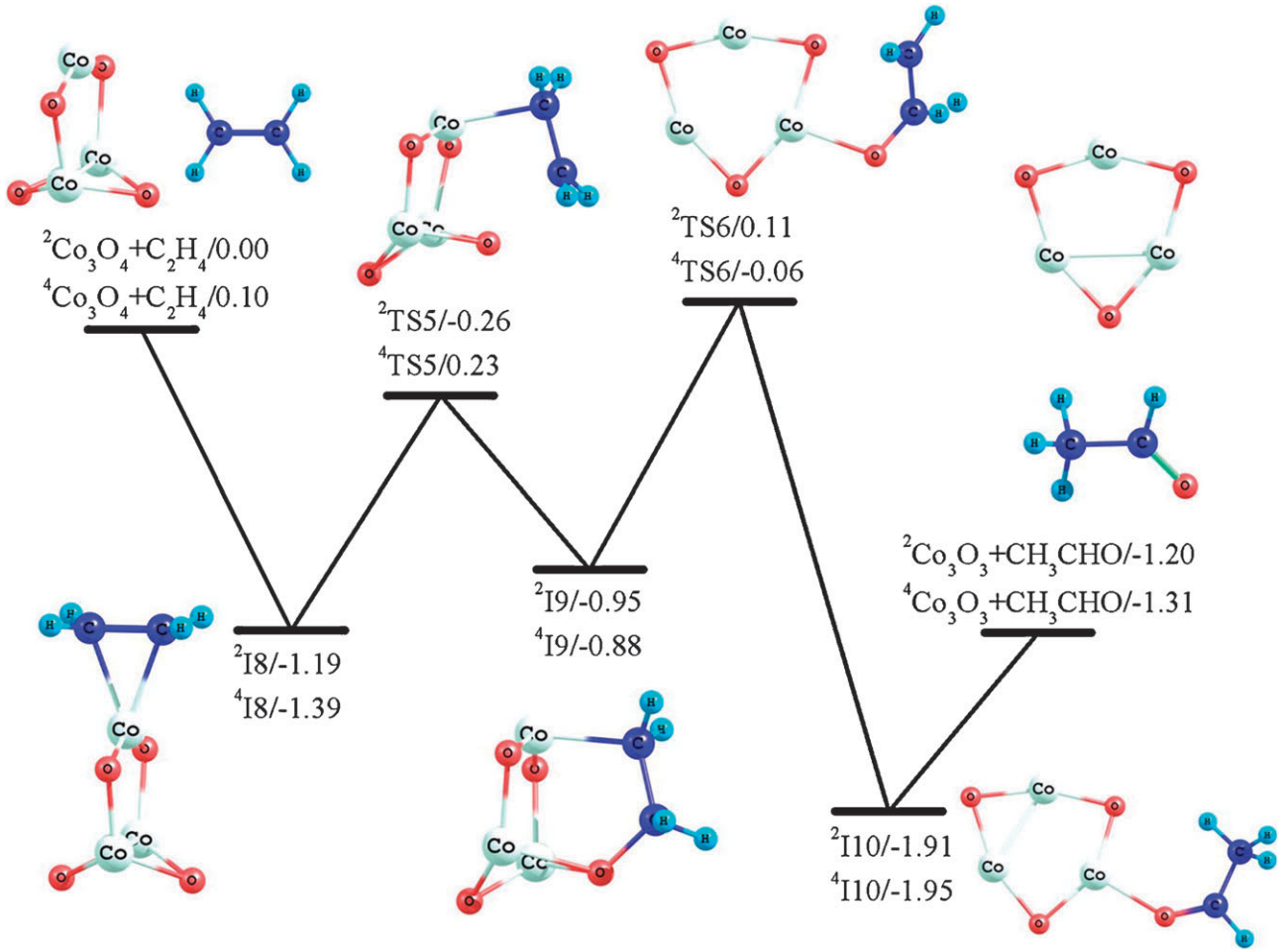

Fig. 8 Reaction pathway for $^{2/4}Co_3O_4 + C_2H_4 \rightarrow {}^{2/4}Co_3O_3 + CH_3CHO$ calculated at the BPW91/TZVP level. See caption to Fig. 4 for explanations. All the energies are relative to the initial energy of the $^2Co_3O_4 + C_2H_4$ reactants.

than the initial energy of $^2Co_3O_4 + C_2H_4$. These differences are small and well within the DFT calculational uncertainties. Note that a spin inversion occurs between **TS5** and **TS6** for the lower energy structure (see Fig. 8).

The observation of cobalt oxide cluster reactivity for the reaction with CO and NO are different from those with C_2H_2 and C_2H_4: the reactivity increases as the cluster size decreases for the former, whereas the reactivity increases as the cluster size increases for the latter. These opposite behaviors with regard to chemical reactivity for Co_mO_n neutral clusters with unsaturated hydrocarbons and the inorganic species CO and NO must be relate to the different nature of the two reaction types and the σ *vs.* π orbital involvement of the bonding interactions. Other small molecules, such as O_2, N_2, N_2O, C_2H_6 and C_3H_8, are examined for the reaction with neutral cobalt oxide clusters, but no reactions are observed for these reactants.

5. Understanding the condensed phase catalytic oxidation reaction by a cobalt oxide catalyst at a molecular level

A redox mechanism by which CO is oxidized to CO_2 and the reduced catalyst is oxidized by gas phase O_2 has been suggested for CO oxidation over a cobalt oxide catalyst.[27c,37,40] Studies for small molecule (CO/NO/C_2H_2/C_2H_4) oxidation catalyzed by neutral cobalt oxide clusters in the gas phase can aid in the understanding of the related condensed phase catalysis reaction at a molecular level. On the basis of experimental and calculational results presented in Fig. 2 and 4, a catalytic cycle for CO oxidation on a cobalt oxide catalyst is proposed and presented in Fig. 9. The proposed mechanism is based on the Mars van Krevelen mechanism;[72] however, the most important information we present for the proposed mechanism is the chemistry of the active sites on the cobalt oxide surface. Compared to other mechanisms based on condensed phase studies, this mechanism indicates that the CO molecule adsorbs on the Co(II) site and reacts with a neighboring oxygen atom, which is bound to an Co(III). The mechanism suggested from condensed phase studies cannot identify the oxidation state of the cobalt atom on which the CO is adsorbed, and previous DFT calculations propose that CO is bound to Co(III). Since both Co(II) and Co(III) exist in the Co_3O_4 cluster, the catalytic cycle shown in Fig. 9 can model the Co_3O_4 catalyst surface behavior. CO molecules can be adsorbed on the Co(II) sites of the cobalt oxide catalyst surface, and CO_2 molecules are formed and dissociated from the surface by reaction of CO with the oxygen atom located on the Co(III) sites. After the reaction, Co(III) is reduced to Co(II).

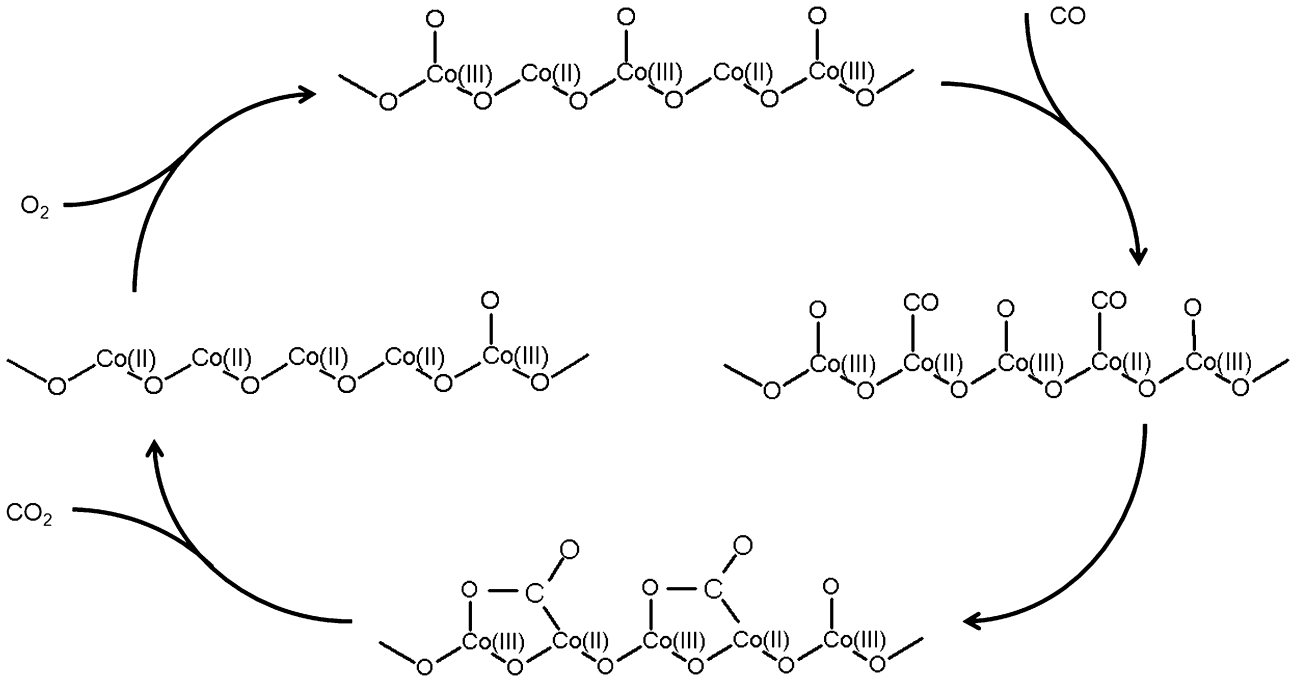

Fig. 9 Proposed full catalytic cycle for CO oxidation to CO_2 on a cobalt oxide surface based on the calculations for the reaction of Co_3O_4 cluster with CO.

The catalyst can be regenerated by reaction with O_2: O_2 molecules dissociate on the catalyst surface and Co(II) sites are re-oxidized to Co(III). The exposed Co(II) sites on the cobalt oxide catalyst surface are the active sites for the CO adsorption; however, pure Co_2O_3, for which only Co(III) sites exist, has no catalytic reactivity toward CO oxidation. In Fig. 9, the processes for CO oxidation and CO_2 desorption from the surface should be thermodynamically favorable, since the gas phase model reaction $CO + Co_3O_4 \rightarrow CO_2 + Co_3O_3$ is calculated as an exothermic reaction and has no reaction barrier (Fig. 4). Additionally, the CO oxidation reaction can occur at low temperature based on the condensed phase studies.[24–41] Regeneration of the catalyst is probably the rate limiting step for the whole catalytic cycle, because the catalyst must be heated to 250 °C or above to be re-oxidized.[27c] According to previous DFT calculations for O_2 adsorption and dissociation on neutral iron oxide clusters,[65a,b] oxidation of metal oxide clusters by O_2 probably involves high reaction barriers, since the strong O–O bond is broken through the oxidation processes. Therefore, dissociation of the O–O bond to form two Co–O bonds is energetically favorable, but with a high barrier. A parallel oxygen bridge is considered to be responsible for the high reactivity of the Co_3O_4 cluster for CO oxidation to CO_2, as discussed above. Oxygen atoms connected to the Co(III) sites and abstracted by CO (Fig. 9) can be suggested to have radical properties based on the gas phase cluster studies: they serve as the active sites, lower CO oxidation reaction barriers, and consequently accelerate CO oxidation to CO_2 in the condensed phase. The catalytic cycle for CO oxidation presented in Fig. 9 can also be operative for the catalytic oxidation reactions of $NO/C_2H_2/C_2H_4$ on a Co_3O_4 surface, as discussed above. This mechanism is based on gas phase cluster studies; however, experimental data and theoretical calculations based on the nanocluster results are in general agreement with the condensed phase conclusions, and therefore help understand the heterogeneous catalytic reaction mechanism on real surfaces.

Conclusions

Reactions of neutral cobalt oxide clusters Co_mO_n with CO, NO, C_2H_2 and C_2H_4 are investigated by time of flight mass spectrometry employing 118 nm single photon ionization and DFT calculations. Strong cluster size dependent behavior is observed for the oxidation reactions of CO, NO, C_2H_2 and C_2H_4 by Co_mO_n clusters (m = 3–9, n = 3–13). This reactivity is associated with the cluster size, appropriate Co(III) concentration, and the number of cobalt atoms with high oxidation states or O–O bonding moieties in the cobalt oxide clusters. The Co_3O_4 cluster has the highest overall rate constants for oxidation of CO and NO; the high reactivity observed for the Co_3O_4 species is in agreement with condensed phase studies. For reactions with C_2H_2 and C_2H_4, clusters with large size, high Co(III) concentration, and a large number of high oxidation state cobalt atoms or O–O bonding moieties have relatively high reactivity. PESs are calculated for these oxidation reactions on the Co_3O_4 cluster, and all the studied molecules are predicted to be adsorbed on the Co(II) site. Additionally, all reactions are estimated as overall barrierless or with a small barrier (<0.23 eV) and thermodynamically favorable processes. Theoretical calculations suggest that the catalytic activity of the Co_3O_4 cluster relates to its unique structure, in which the bridge oxygens, between the two Co(III) atoms, are responsible for the oxidation reactions. A catalytic cycle for CO oxidation on a condensed phase cobalt oxide catalyst surface is proposed based on these gas phase cluster

studies. Such a catalytic cycle can also apply to the oxidation reactions of NO, C_2H_2 and C_2H_4. The re-oxidation of the catalyst by O_2 is suggested to be the rate limiting step in the cyclic process.

Acknowledgements

This work is supported by grants from the U.S. DOE BES program, ASFOR, the NSFERC for Extreme Ultraviolet Science and Technology under NSF Award No. 0310717, and the National Center for Supercomputing Applications under Grant No. CHE080018N and CHE090039.

References

1 J. L. G. Fierro, *Metal Oxides Chemistry and Applications*, Taylor & Francis, Boca Raton, 2006.
2 G. Ertl, H. Knözinger and J. Weitkamp, *Handbook of Heterogeneous Catalysis*, Wiley-VCH, Weinheim, 1997.
3 M. Haruta, S. Tsubota, T. Kobayashi, H. Kageyama, M. J. Genet and B. Delmon, *J. Catal.*, 1993, **144**, 175.
4 (*a*) S. Lee, C. Fan, T. Wu and S. L. Anderson, *J. Am. Chem. Soc.*, 2004, **126**, 5682; (*b*) S. Lee, C. Fan, T. Wu and S. L. Anderson, *J. Chem. Phys.*, 2005, **123**, 124710.
5 D. C. Meier and D. W. Goodman, *J. Am. Chem. Soc.*, 2004, **126**, 1892.
6 T. V. Choudhary and D. W. Goodman, *Appl. Catal., A*, 2005, **291**, 32.
7 T. V. W. Janssens, A. Carlsson, A. Puig-Molina and B. S. Clausen, *J. Catal.*, 2006, **240**, 108.
8 A. S. K. Hashmi and G. J. Hutchings, *Angew. Chem., Int. Ed.*, 2006, **45**, 7896.
9 B. K. Min and C. M. Friend, *Chem. Rev.*, 2007, **107**, 2709.
10 A. A. Herzing, C. J. Kiely, A. F. Carley, P. Landon and G. J. Hutchings, *Science*, 2008, **321**, 1331.
11 (*a*) A. Fielicke, G. von Helden, G. Meijer, B. Simard and D. M. Rayner, *J. Phys. Chem. B*, 2005, **109**, 23935; (*b*) A. Fielicke, G. von Helden, G. Meijer, D. B. Pedersen, B. Simard and D. M. Rayner, *J. Chem. Phys.*, 2006, **124**, 194305.
12 N. Veldeman, P. Lievens and M. Andersson, *J. Phys. Chem. A*, 2005, **109**, 11793.
13 A. Prestianni, A. Martorana, F. Labat, I. Ciofini and C. Adamo, *J. Phys. Chem. B*, 2006, **110**, 12240.
14 (*a*) G. E. Johnson, N. M. Reilly, E. C. Tyo and A. W. Castleman, Jr., *J. Phys. Chem. C*, 2008, **112**, 9730; (*b*) G. E. Johnson, J. U. Reveles, N. M. Reilly, E. C. Tyo, S. N. Khanna and A. W. Castleman, Jr., *J. Phys. Chem. A*, 2008, **112**, 11330.
15 J. S. Walker, G. I. Straguzzi, W. H. Manogue and G. C. A. Schuit, *J. Catal.*, 1988, **110**, 298.
16 M. A. Uddin, T. Komatsu and T. Yashima, *J. Catal.*, 1994, **146**, 468.
17 P. Li, D. E. Miser, S. Rabiei, R. T. Yadav and M. R. Hajaligol, *Appl. Catal., B*, 2003, **43**, 151.
18 Y. Xiong, Z. Li, X. Li, B. Hu and Y. Xie, *Inorg. Chem.*, 2004, **43**, 6540.
19 M. H. Khedr, K. S. A. Halim, M. I. Nasr and A. M. El-Mansy, *Mater. Sci. Eng., A*, 2006, **430**, 40.
20 C. Hu, Z. Gao and X. Yang, *Chem. Lett.*, 2006, **35**, 1288.
21 Y. Zheng, Y. Cheng, Y. Wang, F. Bao, L. Zhou, X. Wei, Y. Zhang and Q. Zheng, *J. Phys. Chem. B*, 2006, **110**, 3093.
22 Á. Szegedi, M. Hegedüs, J. L. Margitfalvi and I. Kiricsi, *Chem. Commun.*, 2005, 1441.
23 H. Lin, Y. Chen and W. Wang, *J. Nanopart. Res.*, 2005, **7**, 249.
24 H. C. Yao and M. Shelef, *J. Phys. Chem.*, 1974, **78**, 2490.
25 (*a*) G. A. El-Shobaky, M. M. Selim and I. F. Hewaidy, *Surf. Technol.*, 1980, **10**, 55; (*b*) G. A. El-Shobaky and N. M. Deraz, *Mater. Lett.*, 2001, **47**, 231.
26 P. Thormählen, M. Skoglundh, E. Fridell and B. Andersson, *J. Catal.*, 1999, **188**, 300.
27 (*a*) J. Jansson, *J. Catal.*, 2000, **194**, 55; (*b*) J. Jansson, M. Skoglundh, E. Fridell and P. Thromählen, *Top. Catal.*, 2001, **16–17**, 385; (*c*) J. Jansson, A. E. Palmqvist, E. Fridell, M. Skoglundh, L. Österlund, P. Thromählen and V. Langer, *J. Catal.*, 2002, **211**, 387.
28 P. Broqvist, I. Panas and H. Persson, *J. Catal.*, 2002, **210**, 198.
29 M. Kang, M. W. Song and C. H. Lee, *Appl. Catal., A*, 2003, **251**, 143.
30 (*a*) H. K. Lin, C. B. Wang, H. C. Chiu and S. H. Chien, *Catal. Lett.*, 2003, **86**, 63; (*b*) H. K. Lin, H. C. Chiu, H. C. Tsai, S. H. Chien and C. B. Wang, *Catal. Lett.*, 2003, **88**, 169.
31 F. Grillo, M. M. Natile and A. Glisenti, *Appl. Catal., B*, 2004, **48**, 267.
32 J. W. Saalfrank and W. F. Maier, *Angew. Chem., Int. Ed.*, 2004, **43**, 2028.
33 M. M. Natile and A. Glisenti, *Chem. Mater.*, 2005, **17**, 3403.
34 Z. Zhang, H. Geng, L. Zheng and B. Du, *J. Alloys Compd.*, 2005, **392**, 317.
35 E. Y. Ko, E. D. Park, H. C. Lee, D. Lee and S. Kim, *Angew. Chem., Int. Ed.*, 2007, **46**, 734.
36 (*a*) M. M. Yung, E. M. Holmgreen and U. S. Ozkan, *J. Catal.*, 2007, **247**, 356; (*b*) M. M. Yung, E. M. Holmgreen and U. S. Ozkan, *Catal. Lett.*, 2007, **118**, 180.
37 M. J. Pollard, B. A. Weinstock, T. E. Bitterwolf, P. R. Griffiths, A. P. Newbery and J. B. Paine, *J. Catal.*, 2008, **254**, 218.
38 Y. Z. Wang, Y. X. Zhao, C. G. Gao and D. S. Liu, *Catal. Lett.*, 2008, **125**, 134.
39 C. Jones, S. H. Taylor, A. Burrows, M. J. Crudace, C. J. Kiely and G. J. Hutchings, *Chem. Commun.*, 2008, 1707.
40 (*a*) J. Y. Luo, M. Meng, X. Li, X. G. Li, Y. Q. Zha, T. D. Hu, Y. N. Xie and J. Zhang, *J. Catal.*, 2008, **254**, 310; (*b*) J. Y. Luo, M. Meng, Y. Q. Zha and L. H. Guo, *J. Phys. Chem.C*, 2008, **112**, 8694.
41 L. F. Liotta, M. Ousmane, G. D. Carlo, G. Pantaleo, G. Deganello, G. Marcí, L. Retailleau and A. Giroir-Fendler, *Appl. Catal., A*, 2008, **347**, 81.
42 C. Chupin, V. M. Konduru, J. Després and C. Mirodatos, *J. Catal.*, 2006, **241**, 103.
43 E. M. Holmgreen, M. M. Yung and U. S. Ozkan, *Appl. Catal., B*, 2007, **74**, 73.
44 J. Yan, M. C. Kung, W. M. H. Sachtler and H. H. Kung, *J. Catal.*, 1997, **172**, 178.
45 A. Y. Khodakov, W. Chu and P. Fongarland, *Chem. Rev.*, 2007, **107**, 1692.
46 J. Gaube and H. F. Klein, *J. Mol. Catal. A: Chem.*, 2008, **283**, 60.
47 C. W. Tang, C. B. Wang and S. H. Chien, *Thermochim. Acta*, 2008, **473**, 68.
48 M. D. Morse, M. E. Geusic, J. R. Heath and R. E. Smalley, *J. Chem. Phys.*, 1985, **83**, 2293.
49 S. Nonose, Y. Sone, N. Kikuchi, K. Fuke and K. Kaya, *Chem. Phys. Lett.*, 1989, **158**, 152.
50 J. Ho, L. Zhu, E. K. Parks and S. J. Riley, *J. Chem. Phys.*, 1993, **99**, 140.
51 M. C. Zonnevylle, J. J. C. Geerlings and R. A. van Santen, *J. Catal.*, 1994, **148**, 417.
52 M. Andersson, J. L. Persson and A. Rosén, *J. Phys. Chem.*, 1996, **100**, 12222.
53 J. L. Rodríguez-López, F. Aguilera-Granja, K. Michaelian and A. Vega, *Phys. Rev. B: Condens. Matter Mater. Phys.*, 2003, **67**, 174413.
54 F. A. Reboredo and G. Galli, *J. Phys. Chem. B*, 2006, **110**, 7979.
55 Y. H. Pan, K. Sohlberg and D. P. Ridge, *J. Am. Chem. Soc.*, 1991, **113**, 2406.
56 A. Nakajima, T. Kishi, Y. Sone, S. Nonose and K. Kaya, *Z. Phys. D, At., Mol. Clusters*, 1991, **19**, 385.
57 B. C. Guo, K. P. Kerns and A. W. Castleman, Jr., *J. Chem. Phys.*, 1992, **96**, 8177.
58 A. M. L. Oiestad and E. Uggerud, *Chem. Phys.*, 2000, **262**, 169.
59 F. Liu, F. X. Li and P. B. Armentrout, *J. Chem. Phys.*, 2005, **123**, 064304.
60 M. Ichihashi, T. Hanmura and T. Kondow, *J. Chem. Phys.*, 2006, **125**, 133404.
61 (*a*) T. Hanmura, M. Ichihashi, Y. Watanabe, N. Isomura and T. Kondow, *J. Phys. Chem. A*, 2007, **111**, 422; (*b*) T. Hanmura, M. Ichihashi and T. Kondow, *Isr. J. Chem.*, 2007, **47**, 37.
62 E. Kapiloff and K. M. Ervin, *J. Phys. Chem. A*, 1997, **101**, 8460.
63 E. L. Uzunova, G. St. Nikolov and H. Mikosch, *J. Phys. Chem. A*, 2002, **106**, 4104.

64 A. Pramann, K. Koyasu, A. Nakajima and K. Kaya, *J. Phys. Chem. A*, 2002, **106**, 4891.

65 (*a*) Y. Xie, F. Dong, S. Heinbuch, J. J. Rocca and E. R. Bernstein, *J. Chem. Phys.*, 2009, **130**, 114306; (*b*) W. Xue, Z. C. Wang, S. G. He, Y. Xie and E. R. Bernstein, *J. Am. Chem. Soc.*, 2008, **130**, 15879; (*c*) S. G. He, Y. Xie, F. Dong, S. Heinbuch, E. Jakubikova, J. J. Rocca and E. R. Bernstein, *J. Phys. Chem. A*, 2008, **112**, 11067; (*d*) F. Dong, S. Heinbuch, Y. Xie, J. J. Rocca, E. R. Bernstein, Z. C. Wang, K. Deng and S. G. He, *J. Am. Chem. Soc.*, 2008, **130**, 1932; (*e*) Y. Xie, S. G. He, F. Dong and E. R. Bernstein, *J. Chem. Phys.*, 2008, **128**, 044306; (*f*) S. G. He, Y. Xie, Y. Q. Guo and E. R. Bernstein, *J. Chem. Phys.*, 2007, **126**, 194315; (*g*) E. Jakubikova and E. R. Bernstein, *J. Phys. Chem. A*, 2007, **111**, 13339; (*h*) Y. Matsuda and E. R. Bernstein, *J. Phys. Chem. A*, 2005, **109**, 3803; (*i*) Y. Matsuda and E. R. Bernstein, *J. Phys. Chem. A*, 2005, **109**, 314; (*j*) Y. Matsuda, D. N. Shin and E. R. Bernstein, *J. Chem. Phys.*, 2004, **120**, 4142; (*k*) Y. Matsuda, D. N. Shin and E. R. Bernstein, *J. Chem. Phys.*, 2004, **120**, 4165; (*l*) D. N. Shin, Y. Matsuda and E. R. Bernstein, *J. Chem. Phys.*, 2004, **120**, 4157; (*m*) E. Jakubikova, A. K. Rappé and E. R. Bernstein, *J. Phys. Chem. A*, 2007, **111**, 12938; (*n*) F. Dong, S. Heinbuch, Y. Xie, J. J. Rocca and E. R. Bernstein, *J. Phys. Chem. A*, 2009, **113**, 3029.

66 M. E. Geusic, M. D. Morse, S. C. O'brien and R. E. Smalley, *Rev. Sci. Instrum.*, 1985, **56**, 2123.

67 A. D. Becke, *Phys. Rev. A: At., Mol., Opt. Phys.*, 1988, **38**, 3098.

68 J. P. Perdew and Y. Wang, *Phys. Rev. B: Condens. Matter*, 1992, **45**, 13244.

69 M. J. Frisch, G. W. Trucks, H. B. Schlegel, G. E. Scuseria, M. A. Robb, J. R. Cheeseman, J. A. Montgomery, Jr., T. Vreven, K. N. Kudin, J. C. Burant, J. M. Millam, S. S. Iyengar, J. Tomasi, V. Barone, B. Mennucci, M. Cossi, G. Scalmani, N. Rega, G. A. Petersson, H. Nakatsuji, M. Hada, M. Ehara, K. Toyota, R. Fukuda, J. Hasegawa, M. Ishida, T. Nakajima, Y. Honda, O. Kitao, H. Nakai, M. Klene, X. Li, J. E. Knox, H. P. Hratchian, J. B. Cross, V. Bakken, C. Adamo, J. Jaramillo, R. Gomperts, R. E. Stratmann, O. Yazyev, A. J. Austin, R. Cammi, C. Pomelli, J. W. Ochterski, P. Y. Ayala, K. Morokuma, G. A. Voth, P. Salvador, J. J. Dannenberg, V. G. Zakrzewski, S. Dapprich, A. D. Daniels, M. C. Strain, O. Farkas, D. K. Malick, A. D. Rabuck, K. Raghavachari, J. B. Foresman, J. V. Ortiz, Q. Cui, A. G. Baboul, S. Clifford, J. Cioslowski, B. B. Stefanov, G. Liu, A. Liashenko, P. Piskorz, I. Komaromi, R. L. Martin, D. J. Fox, T. Keith, M. A. Al-Laham, C. Y. Peng, A. Nanayakkara, M. Challacombe, P. M. W. Gill, B. Johnson, W. Chen, M. W. Wong, C. Gonzalez and J. A. Pople, *GAUSSIAN 03, Revision E.01*, Gaussian, Inc., Wallingford CT, 2004.

70 (*a*) R. C. Bell, K. A. Zemski, K. P. kerns, H. T. Deng and A. W. Castleman, Jr., *J. Phys. Chem. A*, 1998, **102**, 1733; (*b*) R. C. Bell, K. A. Zemski, D. R. Justes and A. W. Castleman, Jr., *J. Chem. Phys.*, 2001, **114**, 798.

71 K. Miaskiewicz and D. A. Smith, *Chem. Phys. Lett.*, 1997, **270**, 376.

72 C. Doornkamp and V. Ponec, *J. Mol. Catal. A: Chem.*, 2000, **162**, 19.